Enhancement of electron correlation due to the molecular dimerization in organic superconductors β-(BDA-TTP)$_2X$ ($X = I_3, SbF_6$)

Hirohito Aizawa*
Institute of Physics, Kanagawa University, Yokohama, Kanagawa 221-8686, Japan

Kazuhiko Kuroki
Department of Physics, Osaka University, Toyonaka, Osaka 560-8531, Japan

Jun-ichi Yamada
Department of Material Science, University of Hyogo, Ako-gun, Hyogo 678-1297, Japan
(Received 5 June 2015; revised manuscript received 10 September 2015; published 7 October 2015)

We perform a first-principles band calculation for quasi-two-dimensional organic superconductors β-(BDA-TTP)$_2I_3$ and β-(BDA-TTP)$_2SbF_6$. The first-principles band structures between the I_3 and SbF_6 salts are apparently different. We construct a tight-binding model for each material which accurately reproduces the first-principles band structure. The obtained transfer energies give the differences as follows: (i) larger dimerization in the I_3 salt than the SbF_6 salt, and (ii) different signs and directions of the interstacking transfer energies. To decompose the origin of the difference into the dimerization and the interstacking transfer energies, we adopt a simplified model by eliminating the dimerization effect and focus only on the difference caused by the interstacking transfer energies. From the analysis using the simplified model, we find that the difference of the band structure comes mainly from the strength of the dimerization. To compare the strength of the electron correlation having roots in the band structure, we calculate the physical properties originating from the effect of the electron correlation such as the spin susceptibility applying the two-particle self-consistent method. We find that the maximum value of the spin susceptibility for the I_3 salt is larger than that of the SbF_6 salt. Hypothetically decreasing the dimerization within the model of the I_3 salt, the spin susceptibility takes almost the same value as that of the SbF_6 salt for the same magnitude of the dimerization. We expect that the different ground state between the I_3 and SbF_6 salt mainly comes from the strength of the dimerization which is apparently masked in the band calculation along a particular k path.

DOI: 10.1103/PhysRevB.92.155108 PACS number(s): 71.15.Mb, 71.10.Fd, 71.20.Rv, 74.70.Kn

I. INTRODUCTION

The organic conductors exhibit a rich variety of physical properties such as spin ordering, charge ordering, Mott insulator, and superconductivity. Modification of the electron correlation, such as by applying the physical pressure, exhibits various phase transitions [1–11]. There have been attempts to synthesize strongly correlated electron systems in organic conductors by applying chemical modifications to stable metallic donor molecules. For example, there are (S,S)-DMBEDT-TTF [12] and *meso*-DMBEDT-TTF [11,13], where two methyl groups are attached to BEDT-TTF, and they produce pressure-induced superconductors. In the present article, we theoretically study superconductors based on the BDA-TTP molecule, which is extended to the six-membered ring from the five-membered ring in the σ-bond framework of the BDH-TTP molecule [7]. The actual materials are β-(BDA-TTP)$_2I_3$ [14] and β-(BDA-TTP)$_2SbF_6$ [15], which will be abbreviated as I_3 and SbF_6 salts, respectively. In both materials, the conductive layer is the BDA-TTP layer, and the anion layer separates the adjacent conductive layers as shown in Fig. 1(a). The molecular configuration in the conductive layer is the β type as shown in Fig. 1(b). Both materials consist of the stacking structure of the BDA-TTP molecules. However, they are somewhat different in that the interstacking direction is slightly tilted in the I_3 salt, but almost side-by-side for the SbF_6 salt, which will be shown later.

The I_3 salt is a Mott insulator [16] at ambient pressure, and the superconductivity appears around 10 K under hydrostatic pressure above 10 kbar [14]. Recently, applying uniaxial strain along the c axis has given higher T_c [17]. It is considered that applying pressure in the I_3 salt increases the overlap between the upper and lower bands, which gradually changes the character of the system from a strongly correlated half-filled system to a moderately correlated quarter-filled system. The c-axis strain more efficiently increases the bandwidth of the overlap. As the electron correlation is reduced to some extent by pressure, the insulating nature of the material is lost, and the superconductivity appears [17]. Theoretically, Nonoyama *et al.* have studied the nature of the charge-ordering state and the pairing mechanisms in the model of the I_3 salt derived from the extended Hückel band structure [18].

The SbF_6 salt exhibits the superconductivity at 7.5 K at ambient pressure [15]. Applying uniaxial compression once increases the T_c and takes a maximum before it decreases [19]. As for the SbF_6 salt, there have been some controversies regarding both the anisotropy of the Fermi surface [20,21] and the directions of the nodes in the superconducting gap [22–25]. In our previous study [26] on β-(BDA-TTP)$_2MF_6$ (M = P, As, Sb, and Ta), we have obtained the band structure from the first-principles band calculation, and suggested the

*aizawa@kanagawa-u.ac.jp

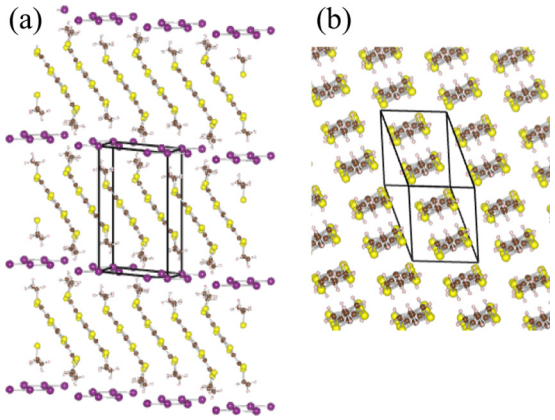

FIG. 1. (Color online) Crystal structure of the I_3 salt from (a) the side view and (b) the conductive layer of the BDA-TTP molecules.

origin of the differences from the extended Hückel band structure [27]. Also, there have been some studies on pairing mechanisms mediated by spin and/or charge fluctuations in the model of β-(BDA-TTP)$_2X$. As for the MF_6 (M = As, Sb) salts, adopting models derived from the extended Hückel calculation, Nonoyama *et al.* [31] have applied the random phase approximation (RPA) to the two-band model, while Suzuki *et al.* [32] have applied the fluctuation-exchange (FLEX) approximation to the original two-band model and the single-band dimer model. Recently, we have constructed the tight-binding model derived from the first-principles band calculation, and studied the pairing symmetry of the gap function within the spin-fluctuation-mediated pairing [26].

In the present study, given the difference in the ground state between the I_3 salt and the SbF_6 salt, we focus on the difference in the electronic structure between the two salts. In fact, despite the similar lattice structure, the band structure of the I_3 salt [14] and that of the SbF_6 salt [15] obtained by the extended Hückel method are known to be very different. Here, we perform the first-principles band calculation for β-(BDA-TTP)$_2I_3$ and construct an effective tight-binding model that reproduces the first-principles band structure. We compare the band structure of the I_3 salt to that of the SbF_6 salt obtained in our previous study [26], and pin down the origin of the apparently large differences. In particular, we study the relation between the strength of the electron correlation and the molecular dimerization. We consider the Hubbard model by introducing the repulsive interaction between the electrons on the same BDA-TTP molecule. Then, we study the effect of the electron correlation by applying the two-particle self-consistent (TPSC) method [33], and present quantities such as the spin susceptibility against the temperature and the dimerization strength, which reflect physical properties originating from the electron correlation. We conclude that the ground state of the I_3 salt differs from that of the SbF_6 salt due to the strength of the dimerization.

This paper is organized as follows. In Sec. II, we present settings of a first-principles band calculation, a model Hamiltonian, and the formulation of the TPSC method. In Sec. III, we present our results of the first-principles band structures (Sec. III A), effective tight-binding models for the I_3 and SbF_6 salts (Sec. III B), discussions from the perspective of simplified models between the two salts (Sec. III C), and effects of the electron correlation (Sec. III D). In Sec. IV, the discussion and conclusion are given.

II. METHOD

A. First-principles band calculation and model construction

We perform a first-principles band calculation using the all-electron full potential linearized augmented plane-wave (LAPW) + local orbitals (lo) method within the framework of WIEN2k [34]. This implements the density functional theory (DFT) with a different possible approximation for the exchange-correlation potentials. The exchange-correlation potential is calculated using the generalized gradient approximation (GGA).

The single-particle wave functions in the interstitial region are expanded by plane waves with a cutoff of $R_{\mathrm{MT}}K_{\mathrm{max}} = 3.0$ due to the presence of the hydrogen atom, where R_{MT} denotes the smallest muffin-tin radius and K_{max} is the maximum value of K vector in the plane-wave expansion. In the I_3 salt, the muffin-tin radii are assumed to be 2.50, 1.62, 1.15, and 0.62 atomic units (a.u.) for I, S, C, and H, respectively. K_{max} is taken as 4.8, and the plane-wave cutoff energy is 318.6 eV. In the SbF_6 salt, the muffin-tin radii are assumed to be 1.74, 1.74, 1.62, 0.83, and 0.45 a.u. for Sb, F, S, C, and H, respectively. K_{max} is taken as 6.7, and the plane-wave cutoff energy is 604.7 eV. Calculations were performed using $6 \times 3 \times 9$ k points for the I_3 salt and $7 \times 3 \times 9$ k points for the SbF_6 salt in the irreducible Brillouin zone. We adopt the lattice structure determined experimentally for each material [14,15], and we do not relax the atomic positions in the calculation.

Having done the first-principles band calculation, we then construct a tight-binding model which accurately reproduces the first-principles band structure. From the lattice structure of the two materials, we regard one molecule as a site and consider a two-band (two sites per unit cell) tight-binding model to fit the first-principles band structure. The tight-binding Hamiltonian, H_0, is written in the form

$$H_0 = \sum_{\langle i\alpha:j\beta\rangle,\sigma} \{t_{i\alpha:j\beta} c^{\dagger}_{i\alpha\sigma} c_{j\beta\sigma} + \mathrm{H.c.}\}, \tag{1}$$

where i and j are unit-cell indices, α and β specify the sites in a unit cell, $c^{\dagger}_{i\alpha\sigma}$ ($c_{i\alpha\sigma}$) is a creation (annihilation) operator with spin σ at the site α in the ith unit cell, $t_{i\alpha:j\beta}$ is the electron transfer energy between the (i,α) site and (j,β) site, and $\langle i\alpha : j\beta\rangle$ represents the summation over bonds corresponding to the transfer.

By Fourier transformation, Eq. (1) is rewritten as

$$H_0 = \sum_{\boldsymbol{k},\sigma,\alpha,\beta} \varepsilon_{\alpha\beta}(\boldsymbol{k}) c^{\dagger}_{\boldsymbol{k}\alpha\sigma} c_{\boldsymbol{k}\beta\sigma}, \tag{2}$$

where $\varepsilon_{\alpha\beta}(\boldsymbol{k})$ is the site-indexed kinetic energy represented in $\boldsymbol{k}$ space. The band dispersion is given by diagonalizing the matrix $\varepsilon_{\alpha\beta}(\boldsymbol{k})$,

$$\varepsilon_{\alpha\beta}(\boldsymbol{k}) = \sum_{\gamma} d_{\alpha\gamma}(\boldsymbol{k}) d^{*}_{\beta\gamma}(\boldsymbol{k}) \xi_{\gamma}(\boldsymbol{k}), \tag{3}$$

where $\xi_\gamma(\boldsymbol{k})$ gives the band dispersion of the γth band measured from the chemical potential, and $d_{\alpha\gamma}(\boldsymbol{k})$ is the unitary matrix that gives the unitary transformation.

We adopt the two-band Hubbard model obtained by adding the on-site (intramolecule) repulsive interaction to the tight-binding model derived from the fitting of the first-principles band structure. The Hubbard Hamiltonian, H, is obtained as

$$H = H_0 + \sum_{i\alpha} U n_{i\alpha\uparrow} n_{i\alpha\downarrow}. \tag{4}$$

Here, the on-site interaction U is considered to contain screening effects from all the other bands that were eliminated when extracting the present model from the first-principles band structure. And $n_{i\alpha\sigma}$ is the number operator of the electron with the spin σ on the α site in the ith unit cell. Since both salts are configured as a form of D_2X where D is the donor molecule and X^{-1} is the anion, the band filling is 1/4-filled in the hole representation (3/4-filled in the electron representation).

B. Two-particle self-consistent method

To deal with effects of the electron correlation arising from the on-site repulsion, we apply TPSC to the multisite Hubbard model given by Eq. (4) as follows. The bare susceptibility in the site representation is given by

$$\chi^0_{\alpha\beta}(q) = -\frac{T}{N_c}\sum_k G^0_{\alpha\beta}(k+q)G^0_{\beta\alpha}(k), \tag{5}$$

where T and N_c are the temperature and the total number of the unit cell, respectively, and $G^0_{\alpha\beta}(k)$ is the bare Green's function given as

$$G^0_{\alpha\beta}(k) = \sum_\gamma d_{\alpha\gamma}(\boldsymbol{k}) d^*_{\beta\gamma}(\boldsymbol{k}) \frac{1}{i\varepsilon_n - \xi_\gamma(\boldsymbol{k})}, \tag{6}$$

where $d_{\alpha\gamma}(\boldsymbol{k})$ is the unitary matrix given in Eq. (3). Here, we introduce the abbreviations $k = (\boldsymbol{k}, i\varepsilon_n)$ and $q = (\boldsymbol{q}, i\omega_m)$ for the fermionic and bosonic Matsubara frequencies. The indices $\alpha\beta$ mean the $(\alpha\,\beta)$ element of the matrix such as $\hat{\chi}^0(q)$.

TPSC has been applied to single-site systems [33,35], multisite systems [36,37], and multiorbital systems [38]. By applying TPSC, we can consider the local vertex correction in both spin and charge channels within a self-consistent procedure. In the TPSC, using the bare susceptibility given by Eq. (5), the spin and charge susceptibilities are obtained as

$$\hat{\chi}^{\rm sp}(q) = [\hat{I} - \hat{\chi}^0(q)\hat{U}^{\rm sp}]^{-1}\hat{\chi}^0(q), \tag{7}$$

$$\hat{\chi}^{\rm ch}(q) = [\hat{I} + \hat{\chi}^0(q)\hat{U}^{\rm ch}]^{-1}\hat{\chi}^0(q), \tag{8}$$

where $\hat{U}^{\rm sp}$ ($\hat{U}^{\rm ch}$) is the local spin (charge) vertex and $\hat{I}$ is the unit matrix. The local vertices are determined by satisfying two sum rules which follow from the fluctuation-dissipation theorem and the Pauli principle for the local moment:

$$\frac{2T}{N_c}\sum_q \chi^{\rm sp}_{\alpha\alpha}(q) = n_\alpha - 2\langle n_{\alpha\uparrow} n_{\alpha\downarrow}\rangle, \tag{9}$$

$$\frac{2T}{N_c}\sum_q \chi^{\rm ch}_{\alpha\alpha}(q) = n_\alpha + 2\langle n_{\alpha\uparrow} n_{\alpha\downarrow}\rangle - n_\alpha^2, \tag{10}$$

where n_α is the particle number at the site α. We have used the relations $n_{\alpha\uparrow} = n_{\alpha\downarrow} = n_\alpha/2$ and $n_{\alpha\sigma} = n^2_{\alpha\sigma}$ from the Pauli principles.

The local spin vertex $\hat{U}^{\rm sp}$ is related to the double occupancy $\langle n_{\alpha\uparrow} n_{\alpha\downarrow}\rangle$ by the following ansatz:

$$U^{\rm sp}_{\alpha\alpha} = \frac{\langle n_{\alpha\uparrow} n_{\alpha\downarrow}\rangle}{\langle n_{\alpha\uparrow}\rangle\langle n_{\alpha\downarrow}\rangle} U_{\alpha\alpha}, \tag{11}$$

where $U_{\alpha\alpha}$ is the $(\alpha\,\alpha)$ element of the on-site interaction matrix $\hat{U}$. Equation (11) breaks the particle-hole symmetry and should be used for $n_\alpha \leqslant 1$. When $n_\alpha > 1$, which can be applied through the particle-hole transformation, then the double occupancy $\langle D_\alpha\rangle = \langle n_{\alpha\uparrow} n_{\alpha\downarrow}\rangle$ is given by

$$\langle D_\alpha\rangle = \frac{U^{\rm sp}_{\alpha\alpha}}{U_{\alpha\alpha}}\frac{n_\alpha^2}{4} + \left(1 - \frac{U^{\rm sp}_{\alpha\alpha}}{U_{\alpha\alpha}}\right)(n_\alpha - 1)\theta(n_\alpha - 1), \tag{12}$$

where $\theta(x)$ is Heaviside step function. Equations (7)–(12) give a set of the self-consistent equations for the TPSC method. Obtaining $\hat{U}_{\rm sp}$ and $\hat{U}_{\rm ch}$, the interaction for the self-energy is obtained as

$$\hat{V}^\Sigma(q) = \tfrac{1}{2}[\hat{U}^{\rm sp}\hat{\chi}^{\rm sp}(q)\hat{U} + \hat{U}^{\rm ch}\hat{\chi}^{\rm ch}(q)\hat{U}]. \tag{13}$$

Using Eq. (13), the self-energy is given by

$$\Sigma_{\alpha\beta}(k) = \frac{T}{N_c}\sum_q V^\Sigma_{\alpha\beta}(q) G_{\alpha\beta}(k-q), \tag{14}$$

and the dressed Green's function is obtained as

$$\hat{G}(k) = [\hat{I} - \hat{G}^0(k)\hat{\Sigma}(k)]^{-1}\hat{G}^0(k). \tag{15}$$

Since we need two sites per unit cell, $\hat{U}$, $\hat{U}^{\rm sp}$, $\hat{U}^{\rm ch}$, $\hat{\chi}^0(q)$, $\hat{\chi}^{\rm sp}(q)$, $\hat{\chi}^{\rm ch}(q)$, $\hat{V}^\Sigma(q)$, $\hat{\Sigma}(k)$, $\hat{G}^0(k)$, and $\hat{G}(k)$ all become 2×2 matrices. In the present study, we adopt the larger eigenvalue of the 2×2 spin-susceptibility matrix as the calculation result of the spin susceptibility. It is a merit of the TPSC method that we can obtain not only the spin susceptibility but also other physical values such as the local spin vertex and the double occupancy. In the present calculation, we take the system size as $64\times 64\,k$ meshes and 16 384 Matsubara frequencies. Since the lowest temperature we calculate in this paper is $T = 0.002$ eV, the energy scale of the Matsubara frequencies for the lowest temperature is about 103 eV.

III. RESULTS

A. First-principles band calculation

Figures 2(a) and 2(c) show the first-principles band structures for the I_3 and SbF_6 salts. For both materials, the experimental lattice structure at ambient pressure and room temperature are used. In both of the materials, it can be seen that the highest-occupied molecular orbital (HOMO) is isolated from the lowest-unoccupied molecular orbital (LUMO). Considering this and also the number of donor molecules in a unit cell, we adopt the HOMO and HOMO − 1 bands as the target bands to construct an effective tight-binding model.

Although only the anion differs, the band structures of the two materials are apparently very different. In order to reveal the origin of this difference in the band structure, we focus on the following two differences of the two salts. One

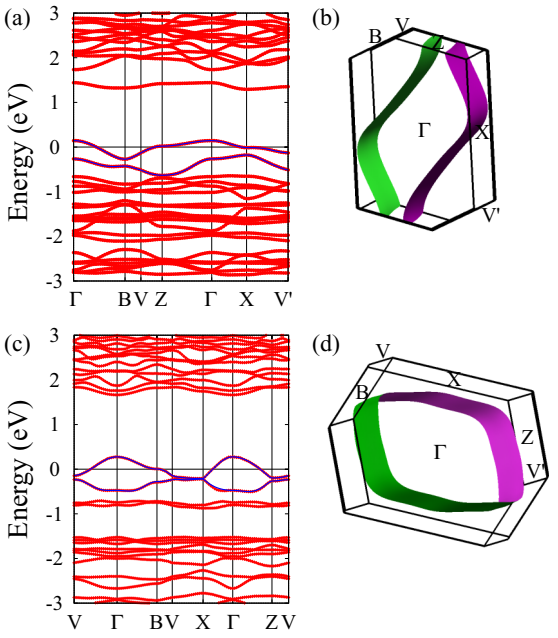

FIG. 2. (Color online) (a) Calculated first-principles band structure and (b) Fermi surface for the I_3 salt; (c) first-principles band structure and (d) Fermi surface for the SbF_6 salt. In both figures of the band structures, the red curves represent the first-principles band structures and the blue solid curves give the tight-binding fit.

is the strength of the molecular dimerization; namely, the dimerization of the donor molecule in the I_3 salt is larger than that in the SbF_6 salt, resulting in a larger gap between HOMO and HOMO $-$ 1 in the former. The other is the anisotropy of the band structure; namely, there are two flat portions near the Fermi level around the Z and the X points in the I_3 salt, while there is only one flat portion around the B point in the SbF_6 salt.

Figure 2(b) shows the Fermi surface of the first-principles band calculation for the I_3 salt, where the high symmetry points in the Brillouin zone are presented only on the $k_Y(k_b) = 0$ plane. The Fermi surface of the I_3 salt is disconnected, namely quasi-one-dimensional, but it is actually close to two-dimensional because a slight shift of the band structure around the Z point would give a closed (i.e., 2D) Fermi surface. Figure 2(d) shows the Fermi surface of the SbF_6 salt. The Fermi surface is cylindrical, reflecting the two-dimensionality of this salt as shown in our previous work [26].

B. Effective tight-binding model

Figure 3 shows the effective tight-binding model adopted to fit the first-principles band. The nearest-neighbor transfers are shown in the left part of Fig. 3, and in addition we also need to introduce the next-nearest-neighbor transfers shown in the right part of Fig. 3 to reproduce the first-principles band structure more accurately. Note that the stacking direction of the BDA-TTP molecules is taken in the a direction [39]. The band dispersions of the tight-binding model are shown as blue solid curves in Fig. 2(a) for the I_3 salt and Fig. 2(c) for the SbF_6 salt, which accurately reproduces the first-principles band structure.

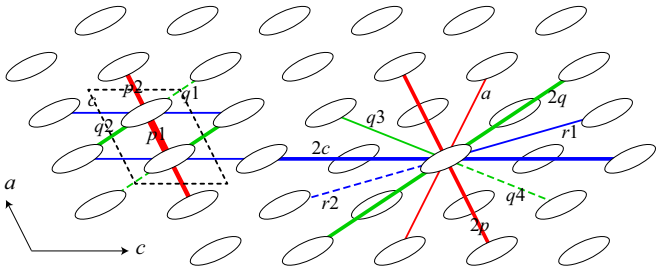

FIG. 3. (Color online) Tight-binding model for β-(BDA-TTP)$_2X$, where left (right) part shows the first (second) nearest neighbor transfer energies. Solid ellipses represent the BDA-TTP molecules and the dashed rectangle is the unit cell.

The transfer energies for the two salts are summarized in Table I. The bottom three lines represent the strength of the dimerization which is measured by the ratio t_{p2}/t_{p1}, and the transfers in the interstacking direction normalized by the average value of the intrastacking transfer energies, $(t_{q1} + t_{q2})/(t_{p1} + t_{p2})$ and $2t_c/(t_{p1} + t_{p2})$. From Table I, it can be seen that there are two major differences between the two salts. One is the strength of the molecular dimerization; namely, the dimerization in the I_3 salt is larger than that in the SbF_6 salt. Another difference is a fact that the transfers along the interstacking directions, namely the magnitude as well as the sign of the interstacking transfers, are different between the two salts, that is, in the c (q) direction in the I_3 (SbF_6) salt.

C. Simplified model eliminating the dimerization

To clarify the origin of the differences between the two salts, we consider the alignment of the donor molecules in the conducting c-a plane for the two salts. The conducting c-a plane for each salt is shown in Fig. 4. We find that the tilting angle of the donor molecules from the c axis is different between the two salts. In the I_3 salt shown in Fig. 4(a), the

TABLE I. List of the transfer energies in units of eV for β-(BDA-TTP)$_2X$.

X	I_3	SbF_6
t_{p1}	−0.174	−0.153
t_{p2}	−0.102	−0.126
t_{q1}	0.018	−0.071
t_{q2}	0.041	−0.055
t_c	0.062	0.007
t_{2c}	0.002	0.005
t_{2p}	0.006	0.021
t_a	−0.001	0.003
t_{2q}	0.004	0.005
t_{q3}	−0.012	0.003
t_{q4}	0.013	0.006
t_{r1}	0.002	0.014
t_{r2}	0.009	0.008
t_{p2}/t_{p1}	0.586	0.824
$\frac{t_{q1}+t_{q2}}{t_{p1}+t_{p2}}$	−0.214	0.452
$\frac{2t_c}{t_{p1}+t_{p2}}$	−0.449	−0.050

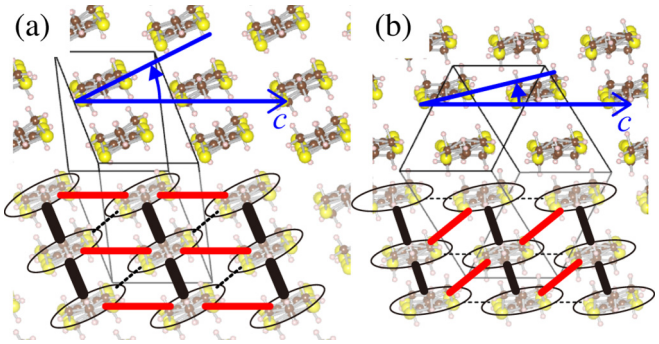

FIG. 4. (Color online) The lattice structures of (a) the I_3 and (b) the SbF_6 salt. Blue solid lines represent the tilting angles of the donor molecules, which is measured from the c direction taken in the horizontal direction. In the lower panel, the ellipses represent the donor molecules, the black solid lines show the intrastacking transfer, and the red solid (black dotted) lines represent the main (not main) interstacking transfer.

tilting angle is larger than that in the SbF_6 salt shown in Fig. 4(b). The difference in the tilting angle gives rise to differences in both the magnitude and the sign of the main interstacking transfers, which is t_c in the I_3 salt shown in the lower panel of Fig. 4(a), while they are t_{q1} and t_{q2} in the SbF_6 salt shown in the lower panel of Fig. 4(b).

Now, let us try to decompose these differences. We consider a case where we hypothetically eliminate the dimerization effect. Namely, we simplify the model by considering only the nearest-neighbor transfer energies, and replace the hopping in the p and q directions by taking their averages. The band structure of the simplified model is given by

$$\varepsilon(\boldsymbol{k}) = 2t_c \cos(k_c) + 2t_p \cos(k_a) + 2t_q \cos(k_c + k_a), \quad (16)$$

where the transfer energies are $t_p = -0.138$ eV, $t_q = 0.030$ eV, $t_c = 0.062$ eV for the I_3 salt, and $t_p = -0.140$ eV, $t_q = -0.063$ eV, $t_c = 0.007$ eV for the SbF_6 salt. Eliminating the dimerization effect enables us to take the unit cell reduced along the a direction. By comparing the band structure of the simplified model between the I_3 and SbF_6 salts, we can focus only on the difference caused by the interstacking transfer.

We compare the band structure of the two salts in the (k_X,k_Y) plane, where k_Y is taken in the molecular stacking direction and k_X is taken in the direction of the main interstacking transfer, namely, the c direction in the I_3 salt [Fig. 5(a)] and the $a/2 + c$ direction in the SbF_6 salt as seen in Fig. 5(b). Also, we shift the wave number by $(\pi,0)$ for the SbF_6 salt considering the sign difference in the main transfer energies along the interstacking direction. By such a transformation, we find that the band structures measured from the Fermi energy between the I_3 salt and the modified SbF_6 salt become very similar as shown in Fig. 5(c). The Fermi surfaces obtained from the simplified model for the two salts are shown in the inset of Fig. 5(c). Since the simplified model eliminates the dimerization effect, the difference in the original band structure between the two salts comes mainly from the dimerization, and the differences coming from the interstacking transfer are not essential.

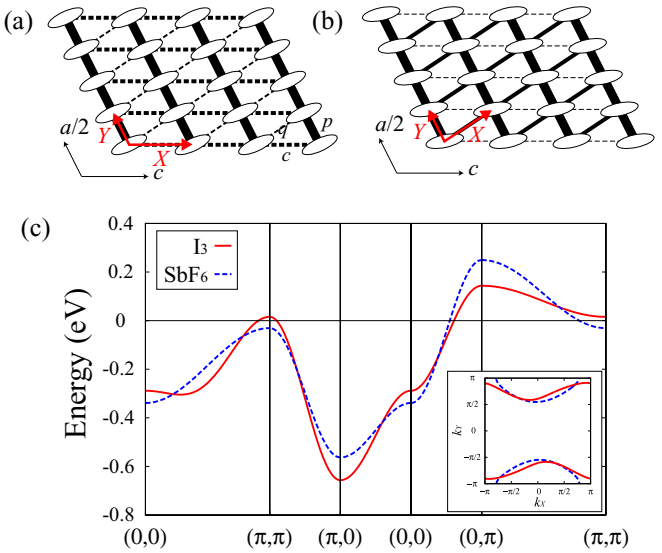

FIG. 5. (Color online) The simplified model for (a) the I_3 salt and (b) the SbF_6 salt, where the linewidth schematically represents the magnitude of the transfer energies, and the solid (dashed) lines represent the negative (positive) value of the transfer energies. (c) The band structures measured from the Fermi energy and an inset shows the Fermi surfaces of the simplified model by eliminating the dimerization for the two salts, where the red solid (blue dashed) curves represent the results of the I_3 (SbF_6) salt.

D. Effect of the electron correlation cooperating with the dimerization

A quarter-filled system effectively becomes a half-filled system by increasing the dimerization [40], so that the electron correlation is strengthened. Since we now know that the strength of the dimerization is the essential difference between the I_3 and SbF_6 salts, we expect that the difference of the ground-state physical properties between the two salts is caused by the strength of the electron correlation originating from the difference in the strength of the dimerization. The strength of the electron correlation can be measured by calculating the double occupancy and spin susceptibility. In fact, it has been shown in a study of organic superconductors κ-(BEDT-TTF)$_2X$ [41] that the magnitude of the band gap far from the Fermi level can drastically affect the spin susceptibility.

We apply the TPSC scheme to the Hubbard model of the I_3 salt. From the first-principles calculation of the I_3 salt, the bandwidth W is about 0.77 eV, so we take the on-site interaction $U = 0.8$ eV as the same as the bandwidth. The on-site interaction U is estimated in the other strongly correlated organic conductors applying the first-principles calculation [42–44]. Referring to them, the on-site interaction we have taken is appropriate.

In the following results, the index α of $U^{\rm sp}_{\alpha\alpha}$, $U^{\rm ch}_{\alpha\alpha}$, and $\langle D_\alpha \rangle$ is omitted since site 1 ($\alpha = 1$) and site 2 ($\alpha = 2$) are equivalent with respect to the rotation around the twofold symmetry axis of the unit cell as seen in Fig. 3. Figure 6(a) shows the temperature dependence of the local vertex of the spin part $U_{\rm sp}$ and the critical on-site interaction of the magnetic order $U_{\rm SDW}$ in the left scale. Above the temperature $T \approx 0.004$ eV, $U_{\rm sp}$ is almost unchanged and $U_{\rm SDW}$ gradually decreases with

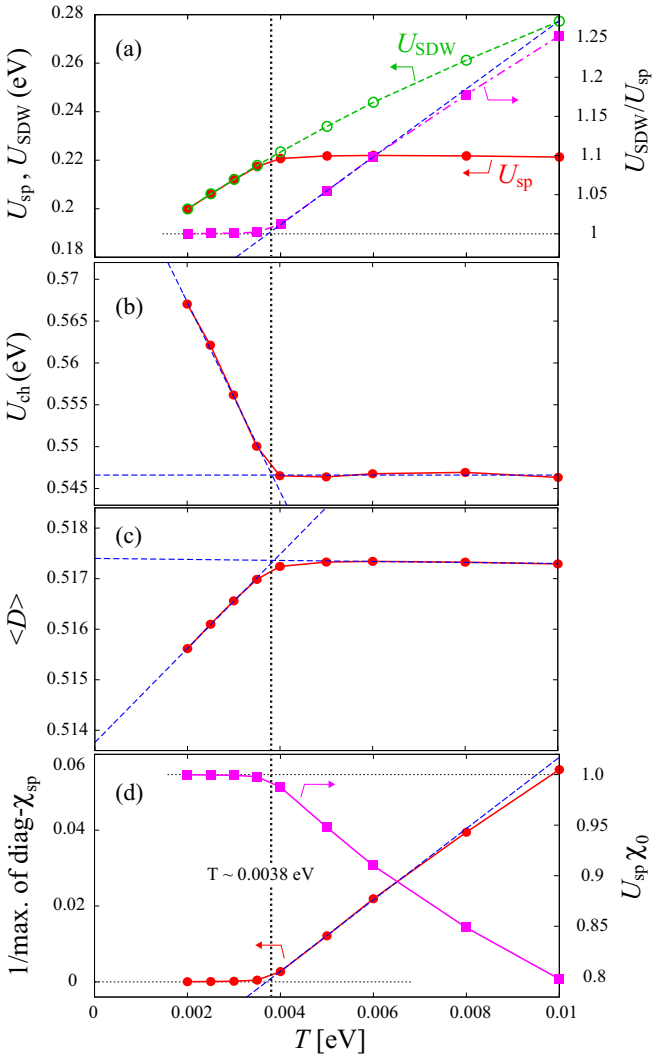

FIG. 6. (Color online) Temperature dependence of (a) U_{sp} and U_{SDW} for the left scale and U_{SDW}/U_{sp} for the right scale, (b) U_{ch}, (c) the double occupancy $\langle D\rangle$, and (d) the inverse of the maximum value of the diagonalized spin susceptibility for the left scale and $U_{sp}\chi_0$ for the right scale in the model of the I_3 salt. Blue dashed lines represent the line extrapolating each value and the black dotted lines are about $T = 0.0038$ eV.

lowering the temperature. Below $T \approx 0.004$ eV, U_{sp} takes almost the same value, but somewhat smaller value than U_{SDW}, which can be understood that the magnetic ordering is developed with lowering the temperature.

In the right scale of Fig. 6(a), we present the ratio U_{SDW}/U_{sp} as a function of T. The TPSC approach satisfies the Mermin-Wagner theorem in two-dimensions [33] so the true magnetic ordering does not occur in the present model, but we can regard the temperature at which the line extrapolating U_{SDW}/U_{sp} from high temperature reaches unity as the magnetic critical temperature in the actual three-dimensional system. We estimate the magnetic critical temperature to be about 0.0038 eV. Reflecting the tendency toward the magnetic ordering, U_{ch} quickly increases below $T = 0.0038$ eV as shown in Fig. 6(b). We show the double occupancy as a function of T in Fig. 6(c). Similarly to the local vertices, the

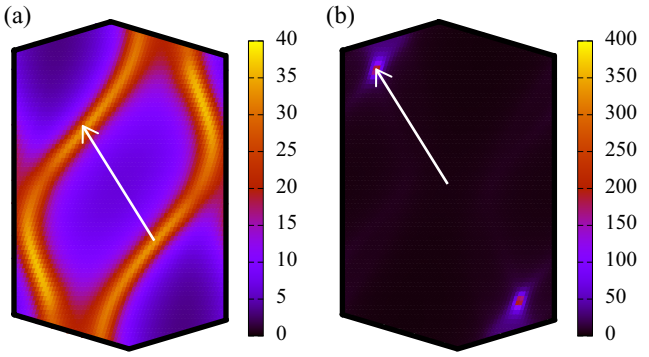

FIG. 7. (Color online) (a) The absolute value of the Green's function and (b) the diagonalized spin susceptibility for the model of the I_3 salt at $T = 0.004$ eV, where the arrow represents the nesting vector.

double occupancy $\langle D\rangle$ also changes below $T = 0.0038$ eV. Decreasing the temperature reduces the double occupancy, which means the magnetic localization develops. The left scale of Fig. 6(d) shows the inverse of the maximum value of the spin susceptibility against T. The right scale of Fig. 6(d) shows the Stoner factor, $U_{sp}\chi_0$, as a function of T. As expected from Fig. 6(a), the inverse of the spin susceptibility extrapolates to zero and the Stoner factor goes to unity around $T = 0.0038$ eV. In fact, a very recent experiment observes a magnetic transition in the Mott-insulating state of the I_3 salt at low temperature [45]. TPSC is not capable of directly describing the magnetic ordering of a Mott insulator, but the very fact that the material is a Mott insulator is consistent with our view that the electron-correlation effect is strong due to the strong dimerization.

Figures 7(a) and 7(b) show the absolute value of the Green's function $|G|$ and the spin susceptibility χ_{sp} of the I_3 salt at $T = 0.004$ eV. The absolute value of the Green's function takes large values near the Fermi surface shown in Fig. 7(a), where the arrow represents the nesting vector of the Fermi surface. The wave number at which the spin susceptibility is maximized corresponds to the nesting vector as shown in Fig. 7(b). As shown in Fig. 7(b), the maximum value of the spin susceptibility takes a large value since its temperature is close to the critical temperature.

To clarify the relation between the electron correlation and the dimerization, we measure the strength of the dimerization by the quantity t_{p2}/t_{p1}. When t_{p2}/t_{p1} goes to unity (t_{p2} goes to t_{p1}), the dimerization decreases. If the decrease of the dimerization results in weakening the electron correlation, we expect (i) U_{sp} gradually deviates from U_{SDW}, (ii) the double occupancy $\langle D\rangle$ becomes large, and (iii) the maximum value of the spin susceptibility decreases within the TPSC scheme. Furthermore, if the stronger electron correlation of the I_3 salt originates from the stronger molecular dimerization, all the quantities should approach the values close to those of the SbF_6 salt when the dimerization is reduced hypothetically in the model of the I_3 salt.

Let us now investigate the relation between the dimerization and the electron correlation. Figure 8(a) shows the local vertex of the spin part U_{sp} and the critical on-site interaction for the magnetic order U_{SDW} as functions of t_{p2}/t_{p1} for the model of the I_3 salt with $T = 0.004$ eV. The results for the SbF_6 salt

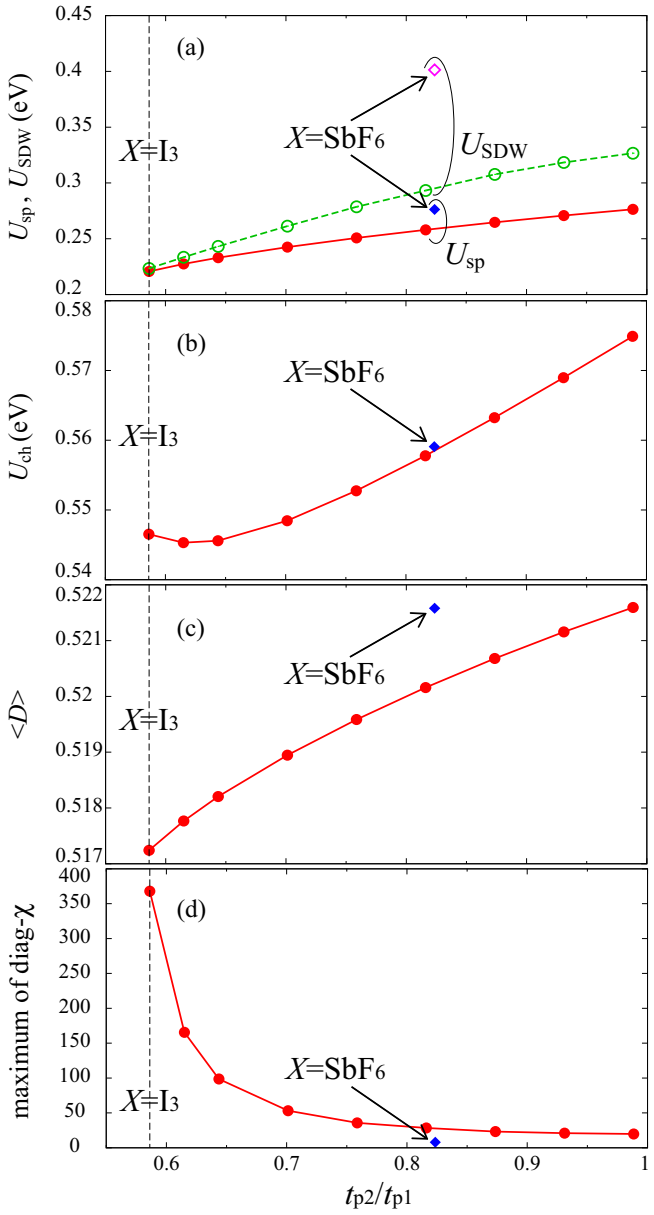

FIG. 8. (Color online) The strength of the dimerization t_{p2}/t_{p1} dependence of (a) $U_{\rm sp}$ and $U_{\rm SDW}$, (b) $U_{\rm ch}$, (c) the double occupancy $\langle D\rangle$, and (d) the maximum value of the diagonalized spin susceptibility for the model of the I_3 salt with $U = 0.8$ eV and $T = 0.004$ eV. The results obtained for the model of the SbF_6 salt with the same U and T are also shown by the diamonds (indicated by the arrows) at the value of t_{p2}/t_{p1} of the SbF_6 salt, and in (a), the solid blue (open purple) diamonds correspond to $U_{\rm sp}$ ($U_{\rm SDW}$).

are also shown at the corresponding value of t_{p2}/t_{p1}. As the dimerization is decreased (t_{p2}/t_{p1} is increased), $U_{\rm sp}$ gradually deviates from $U_{\rm SDW}$, which indicates that increasing t_{p2}/t_{p1} suppresses the maximum value of the spin susceptibility. As for local vertex of the charge part, in contrast to its temperature dependence [shown in Fig. 6(b)], decreasing the dimerization increases $U_{\rm ch}$ as seen in Fig. 8(b), although $U_{\rm sp}$ deviates from $U_{\rm SDW}$ similarly to its temperature dependence shown in Fig. 6(a). In Fig. 8(c), it can be seen that the double occupancy $\langle D\rangle$ monotonically increases with decreasing the dimerization, which can be understood as the suppression of the magnetic localization. This tendency is confirmed by the deviation of $U_{\rm sp}$ from $U_{\rm SDW}$. Figure 8(d) shows the maximum value of the spin susceptibility as a function of t_{p2}/t_{p1}. Decreasing the dimerization from the actual value of the I_3 salt quickly suppresses the spin susceptibility, and that of the I_3 salt takes almost the same value as that of the SbF_6 salt around the same strength of the dimerization.

From the t_{p2}/t_{p1} dependence in Fig. 8, we can say that the electron correlation in the I_3 salt is stronger than in the SbF_6 salt due to the strong dimerization. We therefore conclude that the difference of the ground state between the two salts, namely, insulating for the I_3 salt and superconducting for the SbF_6 salt, originates from the strength of the dimerization, which affects the electron correlation. Applying pressure to the I_3 salt reduces the dimerization, resulting in the metallicity, and hence the superconductivity appears.

IV. CONCLUSION

In the present study, we have performed first-principles band calculations and have derived the effective tight-binding models of β-(BDA-TTP)$_2I_3$ and β-(BDA-TTP)$_2SbF_6$. The band structure and the Fermi surface between the I_3 and SbF_6 salts are apparently different although only the anion differs. The derived tight-binding models, which accurately reproduce the first-principles band structures of the two salts, show that the differences between the two salts comes mainly from the strength of the dimerization.

As for the effect of the electron correlation, we have presented the TPSC results for quantities such as the spin susceptibility in the Hubbard model for the two salts. The TPSC results show that the electron correlation becomes stronger upon lowering the temperature. Then, we have hypothetically reduced the strength of the dimerization in the I_3 salt to that of the SbF_6 salt, where all the calculated quantities tend to become similar to those of the SbF_6 salt. Thus, we conclude that the electron correlation in the I_3 salt is stronger than the SbF_6 salt due to the strong dimerization. The expected stronger correlation in the I_3 salt is at least qualitatively consistent with a recent experimental observation that the material is a Mott insulator, which is a hallmark of strong correlation, and exhibits a magnetic transition at low temperature [45]. Applying pressure to the I_3 salt reduces the dimerization, which weakens the electron correlation, and hence the superconductivity appears as in the SbF_6 salt.

In the present study, we have considered only the on-site (intramolecular) electron-electron interaction. It remains an interesting future problem to study the effect of the off-site (intermolecular) interactions. In fact, it has been known that in organic conductors having quarter-filled bands, the Mott-insulating state often competes with the charge ordering and/or charge-density-wave states [46]. It is an interesting issue to investigate how such interactions would affect the insulating properties as well as the mechanism of the superconductivity.

ACKNOWLEDGMENTS

We thank T. Isono for showing the latest experimental data. This work is supported by a Grant-in-Aid for Scientific

Research from the Ministry of Education, Culture, Sports, Science, and Technology of Japan (Grant No. 20110007). Part of the calculation has been performed at the facilities of the Supercomputer Center, ISSP, University of Tokyo.

[1] T. Ishiguro, K. Yamaji, and G. Saito, *Organic Superconductors* (Springer, Heidelberg, 1998), 2nd ed.
[2] C. Bourbonnais and D. Jérome, *Advances in Synthetic Metals, Twenty Years of Progress in Science and Technology* (Elsevier, New York, 1999).
[3] M. Lang and J. Müller, *The Physics of Superconductors*, Vol. 2 (Springer-Verlag, Heidelberg, 2003).
[4] For a review, Chem. Rev. **104**(11) (2004), special issue on molecular conductors.
[5] T. Mori, Chem. Rev. **104**, 4947 (2004).
[6] H. Seo, C. Hotta, and H. Fukuyama, Chem. Rev. **104**, 5005 (2004).
[7] J. Yamada, H. Akutsu, H. Nishikawa, and K. Kikuchi, Chem. Rev. **104**, 5057 (2004).
[8] For a review, J. Phys. Soc. Jpn. **75**(5) (2006), special topics, organic conductors.
[9] For a recent review, Crystals **2**-**3** (2012), special issue on molecular conductors.
[10] J. Yamada and H. Akutsu, Crystals **2**, 812 (2012).
[11] T. Shikama, T. Shimokawa, S. Lee, T. Isono, A. Ueda, K. Takahashi, A. Nakao, R. Kumai, H. Nakao, K. Kobayashi, Y. Murakami, M. Kimata, H. Tajima, K. Matsubayashi, Y. Uwatoko, Y. Nishio, K. Kajita, and H. Mori, Crystals **2**, 1502 (2012).
[12] J. S. Zambounis, C. W. Mayer, K. Hauenstein, B. Hilti, W. Hofherr, J. Pfeiffer, M. Bürkle, and G. Rihs, Adv. Mater. **4**, 33 (1992).
[13] S. Kimura, T. Maejima, H. Suzuki, R. Chiba, H. Mori, T. Kawamoto, T. Mori, H. Moriyama, Y. Nishio, and K. Kajita, Chem. Commun. **2004**, 2454 (2004).
[14] J. Yamada, K. Fujimoto, H. Akutsu, S. Nakatsuji, A. Miyazaki, M. Aimatsu, S. Kudo, T. Enoki, and K. Kikuchi, Chem. Commun. **2006**, 1331 (2006).
[15] J. Yamada, M. Watanabe, H. Akutsu, S. Nakatsuji, H. Nishikawa, I. Ikemoto, and K. Kikuchi, J. Am. Chem. Soc. **123**, 4174 (2001).
[16] M. Uruichi, C. Nakano, M. Tanaka, K. Yakushi, T. Kaihatsu, and J. Yamada, Solid State Commun. **147**, 484 (2008).
[17] K. Kikuchi, T. Isono, M. Kojima, H. Yoshimoto, T. Kodama, W. Fujita, K. Yokogawa, H. Yoshino, K. Murata, T. Kaihatsu, H. Akutsu, and J. Yamada, J. Am. Chem. Soc. **133**, 19590 (2011).
[18] Y. Nonoyama, Y. Maekawa, A. Kobayashi, Y. Suzumura, and J. Yamada, J. Phys.: Conf. Ser. **132**, 012013 (2008).
[19] H. Ito, T. Ishihara, H. Tanaka, S.-I. Kuroda, T. Suzuki, S. Onari, Y. Tanaka, J.-I. Yamada, and K. Kikuchi, Phys. Rev. B **78**, 172506 (2008).
[20] E. S. Choi, E. Jobilong, A. Wade, E. Goetz, J. S. Brooks, J. Yamada, T. Mizutani, T. Kinoshita, and M. Tokumoto, Phys. Rev. B **67**, 174511 (2003).
[21] S. Yasuzuka, H. Koga, Y. Yamamura, K. Saito, S. Uji, T. Terashima, H. Aizawa, K. Kuroki, M. Tsuchiizu, H. Akutsu, and J. Yamada, J. Phys. Soc. Jpn. **81**, 035006 (2012).
[22] Y. Shimojo, T. Ishiguro, T. Toita, and J. Yamada, J. Phys. Soc. Jpn. **71**, 717 (2002).
[23] M. A. Tanatar, T. Ishiguro, T. Toita, and J. Yamada, Phys. Rev. B **71**, 024531 (2005).
[24] K. Nomura, R. Muraoka, N. Matsunaga, K. Ichimura, and J. Yamada, Physica B **404**, 562 (2009).
[25] S. Yasuzuka (private communication).
[26] H. Aizawa, K. Kuroki, S. Yasuzuka, and J. Yamada, New J. Phys. **14**, 113045 (2012).
[27] Recently, several studies report that the first-principles band structure slightly differs from that obtained by the extended Hückel method [28–30].
[28] H. C. Kandpal, I. Opahle, Y.-Z. Zhang, H. O. Jeschke, and R. Valenti, Phys. Rev. Lett. **103**, 067004 (2009).
[29] Y. Nagai, H. Nakamura, and M. Machida, Phys. Rev. B **83**, 104523 (2011).
[30] P. Alemany, J.-P. Pouget, and E. Canadell, Phys. Rev. B **89**, 155124 (2014).
[31] Y. Nonoyama, Y. Maekawa, A. Kobayashi, Y. Suzumura, and H. Ito, J. Phys. Soc. Jpn. **77**, 094703 (2008).
[32] T. Suzuki, S. Onari, H. Ito, and Y. Tanaka, J. Phys. Soc. Jpn. **80**, 094704 (2011).
[33] Y. M. Vilk and A.-M. S. Tremblay, J. Phys. I (France) **7**, 1309 (1997).
[34] P. Blaha, K. Schwarz, G. K. H. Madsen, D. Kvasnicka, and J. Luitz, *WIEN2k, An Augmented Plane Wave + Local Orbitals Program for Calculating Crystal Properties* (Karlheinz Schwarz/ Technische Universität Wien, Wien, Austria, 2001).
[35] J. Otsuki, Phys. Rev. B **85**, 104513 (2012).
[36] S. Arya, P. V. Sriluckshmy, S. R. Hassan, and A.-M. S. Tremblay, Phys. Rev. B **92**, 045111 (2015).
[37] D. Ogura and K. Kuroki, arXiv:1505.04017.
[38] H. Miyahara, R. Arita, and H. Ikeda, Phys. Rev. B **87**, 045113 (2013).
[39] For the correspondence with our previous study [26], the lattice coordinates as the c and a taken in the SbF_6 salt correspond with the $-c$ and $c+a$ in the I_3 salt according to the structure data for both materials [14,15]. Similarly, the notation of the transfer energies is different. We employ the lattice coordinates and notation of the I_3 salt in this article.
[40] H. Kino and H. Fukuyama, J. Phys. Soc. Jpn. **65**, 2158 (1996).
[41] K. Kuroki, T. Kimura, R. Arita, Y. Tanaka, and Y. Matsuda, Phys. Rev. B **65**, 100516 (2002).
[42] L. Cano-Cortés, A. Dolfen, J. Merino, J. Behler, B. Delley, K. Reuter, and E. Koch, Eur. Phys. J. B **56**, 173 (2007).
[43] K. Nakamura, Y. Yoshimoto, T. Kosugi, R. Arita, and M. Imada, J. Phys. Soc. Jpn. **78**, 083710 (2009).
[44] K. Nakamura, Y. Yoshimoto, and M. Imada, Phys. Rev. B **86**, 205117 (2012).
[45] T. Isono (private communication).
[46] For a review, H. Seo, J. Merino, H. Yoshioka, and M. Ogata, J. Phys. Soc. Jpn. **75**, 051009 (2006).